Supporting Oxides on Charcoal via Wet Impregnation for Nitrate Removal from Water

By

Leonel A. Long [1], Pablo M. Arnal [1,2] *

1 Centro de Tecnología de Recursos Minerales y Cerámica (CETMIC), Camino Centenario y 506, CC 49, B1897ZCA, M. B. Gonnet – La Plata, Argentina.

2 Facultad de Ciencias Exactas, Universidad Nacional de La Plata. 47 y 115 (1900) La Plata, Argentina

Corresponding Author

* E-mail: arnal@química.unlp.edu.ar

Highlights

- M-oxides (M = Al, Fe, Mg, Zn) incorporates into charcoal via wet impregnation.
- Charcoal-supported zinc oxide outperforms charcoal without oxide.
- Carbonaceous matrix loses significant mass though keeps pore structure.
- Charcoal´s role in nitrate removal requires further investigation.

Abstract

This work investigates the synthesis of M-oxides (M = aluminum, iron, magnesium, zinc) supported on charcoal by wet impregnation and using these materials in removing nitrate from water. On the one hand, it studies the incorporation of the solid and the modification that the carbonaceous support undergoes, and on the other hand, it investigates the performance of the material produced in the synthesis compared to charcoal acting as a control group. In the first part, the incorporation of the solid material was characterized structurally (SEM, Hg porosimetry) and compositionally (XRD, elemental analysis), and the modification of the carbonaceous support was characterized by the yield and the amount of solid incorporated in the synthesis product (TGA). The results show that the synthesis by wet impregnation produces a composite material formed by a porous matrix of carbon-containing solid in an amount, with a distribution and precursor-dependent crystallinity. The synthesis also results in the loss of a significant amount of carbonaceous support, which varies from precursor to precursor. The results also show that only the material with zinc oxide outperforms the material with no added solid in removing nitrate from water. Finally, this work´s results show that wet impregnation allows obtaining materials that improve the ability to remove nitrate from water. However, they show that the carbonaceous support undergoes a significant change whose influence on nitrate removal remains unknown.

Key Words: Charcoal, Biochar, Oxide, Nitrate removal, Wet impregnation.

1. Introduction

Water filters attract scientist´s interest worldwide. Particularly, charcoal-based filters stand out because they operate with simple and established technology. Charcoal is a carbon-rich solid formed by thermal treatment of plant biomass in a non-oxidizing atmosphere. Its open pore structure enables the mass transfer of water within the particle. The inner surface has diverse oxygen-containing functional groups. Charcoal´s ability to bind to cations (Lewis acids [1]) and to retain them explains its usefulness in water filtration [2][3][4][5][6].

Charcoal´s ability to remove cations from water contrasts with its inability to remove anions (Lewis bases [1]). To filter anions from water with charcoal filters, scientists have modified the synthesis of charcoal to create a surface with chemical groups that have an affinity for anionic contaminants. For nitrate filtration, two strategies have received particular attention: (a) modification of the chemical groups on the surface and (b) addition of particles of other material in the pores [7]. In the latter, however, it is poorly understood how incorporating another material modifies the support (charcoal) and how those materials remove nitrate.

In this work, we synthesized charcoal-supported oxides (of aluminum, iron, magnesium, or zinc) via wet-impregnation, characterized those materials, and investigated how they remove nitrate from water. We hypothesized that oxides form onto charcoal (support) via wet impregnation and that those materials outperform charcoal used as support in removing nitrate. To carry out this work, we used charcoal prepared from Eucalyptus wood. Charcoal´s ability to remove nitrate from water was tested in batch systems.

2. Materials and Methods

2.1 Materials

Nitric acid (65% w/w) and hydrochloric acid (36.5-38.0% w/w) were purchased from Cicarerlli. Aluminum acetate was purchased from Fisher Scientific Company, and magnesium carbonate from BDH. Iron nitrate nona-hydrate, zinc chloride and potassium nitrate were all purchased from Biopack. Potassium nitrate solution was prepared by dissolving KNO_3 (1.6599 g, dried at 110 °C, 24 h) in 500.00 mL of distilled water (2036 ± 4 mg $NO_3^-.L^{-1}$). Solutions of lower concentration were obtained by dilution. Nitrate concentration was determined spectrophotometrically (UV-Vis, ASTM 4500-NO_3^- B).

Acid-treated charcoal (C*) was prepared as previously reported [8]. Shortly, as made charcoal (34.1 g) was dispersed in HNO_3 (225 mL) in a beaker (500 mL) covered with watch glass. The beaker was heated in a water bath at 80°C for 3 hours. The dispersion was stirred intermittently with a glass rod for a few seconds every 30 minutes. Then, the solid was separated by filtration and washed with distilled water until the eluent´s pH matched the pH of the distilled water. Afterwards, the solid was dispersed in water (250 mL) in a glass beaker (500 mL). The dispersion was boiled 3 h, cooled to room temperature and left on the bench 24 h. The solid was recovered by filtration and washed with distilled water until the eluent´s pH matched the pH of the distilled water. The solid was dried in an oven (60 °C, 72 h).

2.2 Synthesis of C*M800 (M = Al, Fe, Mg, Zn)

The starting material, **C***, underwent a two-step process to form **C*M800** (M = Al, Fe, Mg, Zn) (Scheme 1). First, the precursor **C*** was wet-impregnated with the M precursor to produce the material **C*M**.

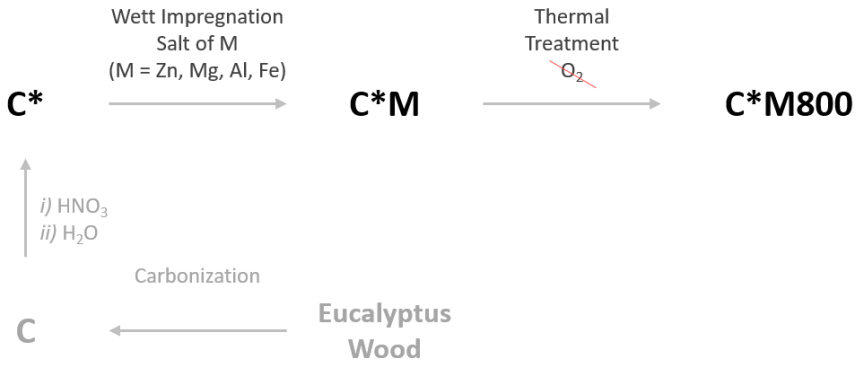

Scheme 1. Scheme for converting charcoal treated with nitric acid (**C***) into composite material (**C*M800**) through wet impregnation with M-metal salt, followed by heat treatment in a non-oxidizing atmosphere.

C* (4.0000 g) was dispersed in a solution of the metal precursor (see Table 1). The dispersion was magnetically stirred (room temperature, 18 h). After recovering by filtration, the solid was oven dried (60°C, 72 h).

Table 1. Solutions that were utilized to wet-impregnate **C*** with M-precursors.

Precursor		*Solvent*	
Type	*(g)*	*Type*	*(mL)*
$ZnCl_2$	30.0749	Water	250
$Al(Ac)_3$	12.0000	Water	150
$Fe(NO_3)_3$	30.0749	Water	150

$Mg(CO_3)$	91.0538	HCl	175

Next, **C*M** was heat-treated in a non-oxidizing atmosphere (as we previously described [9]) to form **C*M800**. Briefly, the impregnated charcoal (ca. 4 g) was heat treated (RT - 800 °C, 10 °C.min^{-1}; 800 °C, 3 h; oven cooled to RT) in a self-made ceramic vessel.

2.3 Characterizations of C*M800

Scanning Electron Microscopy. Dried particles (110 °C, 24 h) were analyzed with a scanning electron microscope (JEOL JCM-6000 Neo Scope, High-vaccum, PC-High 15 kV).

Hg Porosimmetry. The powder was dried (110 °C, 24 h) before measuring Hg porosimetry isotherms (Pascal-Thermo Fisher Module 440 & Module 140). Accumulated specific pore volumes were calculated (SOL.I.D software) between 10 nm and 100 µm. The pore size distribution was calculated from the derivative of the accumulated specific pore volume. Macropore volume was estimated directly from the intrusion isotherm curve.

X-Ray Diffraction (XRD). Diffractograms were obtained from dried powders (Philips PW-3710; Cu-Kα radiation λ = 0.154 nm, 35 kV, 40 mA, step 0.04°, 2 s.step^{-1}). Reflexes were assigned after comparing the diffractogram with reflexes from a database (Open Crystallographic Database, http://www.crystallography.net/cod/, software X'Pert HighScore).

Energy-dispersive X-ray Fluorescence (EDX). Dried impregnated charcoals as well as ashes obtained from thermal gravimetric analysis were analyzed with EDX (JEOL JCM-6000 Neo Scope) to obtain an elemental composition and mapping of elements.

Elemental Analysis CHN. The **C*Zn800** dried powder was analyzed with Elemental Analysis equipment (CE 440 – Exeter). Calibration was carried out with acetanilide patron. Results was expressed in element percentage.

Thermal Gravimetric Analysis (TGA). Amount of solid incorporated via wet impregnation in charcoal was estimated from the mass of ashes obtained after burning the impregnated charcoals (Rigaku Thermo Plus II; drying 100 °C 2 h, 100 to 1000 °C at 10 °C.min^{-1} under airflow).

2.4 Removal of Nitrate by C*M800

The nitrate removal capacity of **C*M800** charcoals (M = Zn, Mg, Fe, and Al) was studied in batch systems (30 g.L-1 or 10 g.L-1 ; 24 h). For S/L = 30 g.L-1 , 100 mg of **C*M800** were dispersed in 10 mL of nitrate solution (105 ± 3 ppm) inside a Falcon tube (15 mL, screw-capped). For S/L = 10 g.L-1 , 150 mg of **C*M800** were dispersed in 5 mL of nitrate solution (93.2 ± 0.7 ppm). Falcon tubes were kept on rotary shaker at 25 °C for 24 h. Then, the solid was separated by centrifugation (10.000 rpm,15 min, Centrifuge Presvac, EPF-12 model) and the liquid´s nitrate content was quantified spectrophotometrically (HP 8453, 220 nm).

2.5 Nitrate Removal Kinetics and Isotherms of C*Zn800

Kinetics of nitrate removal by C*Zn800. The ability of **C*Zn800** to remove nitrate from solution was investigated in batch systems at either 10 or 30 g.L^{-1} solid-liquid ratio starting at about 100 ppm nitrate. 10 g.L^{-1} solid-liquid ratio systems were obtained by adding 150 mg of **C*Zn800** in 5 mL of nitrate solution on a 15 mL plastic conical centrifuge tube with screw cap. 30 g.L^{-1} solid-liquid ratio systems were obtained by adding 15 mg of **C*Zn800** in 5 mL of nitrate solution (20.0 ± 0.2 y 2036 ± 4 ppm) on similar tubes. Closed tubes were mechanically agitated (Decalab Rotolab-25, 25 °C) for

24 h. After filtration, the concentration of nitrate in aqueous solution was determined spectrophotometrically (HP 8453, 220 nm). All experiments were done in triplicate.

Isotherm of Nitrate Removal by C*Zn800. To obtain nitrate adsorption isotherms, batch systems (30 $g.L^{-1}$) were prepared by dispersing 150 mg of **C*Zn800** in 5 mL of nitrate solution (20.0 ± 0.2; 105 ± 3; 200 ± 1; 1008 ± 5; and 2036 ± 4) in 15 mL Falcon tubes with lids. After stirring mechanically all tubes (Decalab Rotolab 25 rotary shaker, 5 h), the liquid was recovered by filtration (nitrocellulose filters) and its nitrate concentration was measured spectrophotometrically (see above).

2.6 Numerical Methods

Yield of synthesis and Calculation of C mass loss. The synthesis yield of **C*M800** was calculated as the mass of product formed per 100 g of charcoal used as support (**C*** in this case) (see Figure 1).

The percentage mass loss of the **C*** support (Δm) was calculated using the following equation.

$$\Delta m = 100 - \left(\frac{Yield * (100 - Ashes)}{100}\right) \quad (1)$$

In 100 g of **C*M800**, there are X g of incorporated solid (which we estimate from the ash obtained from the combustion of **C*M800**) and there are 100 - X g of charcoal (we assume that the material being burned is charcoal). Thus, for a mass of **C*M800** equal to the yield, there is a mass of charcoal equal to

$$\left(\frac{Yield * (100 - Ashes)}{100}\right) \quad (2)$$

The mass loss can therefore be estimated as 100 g minus the mass of charcoal remaining in **C*M800** (see Figure 1).

Nitrate Removal Experiments. *Mean Values*. Mean values were calculated from three independent experiments and expressed as mean value ± confidence interval (CI) obtained from ANOVA.

Comparison of Mean Values with ANOVA. Analysis of variance (ANOVA) of ΔpH and C_e of nitrate was conducted (InfoStat version 2020; Centro de Transferencia InfoStat, FCA, Universidad Nacional de Córdoba, Argentina) (α = 0.05). Data normality was verified with a Q-Q plot. Variance homogeneity was verified with the scatter plot of residuals of variables (see SI section D).

Pair-wise Comparison of Mean Values with Tukey Test. Comparisons among multiple means were made by the Tukey test (α = 0.05).

Kinetics of nitrate removal by ***C*Zn800***. The kinetic data were calculated with the equation (3)

$$q_t = \frac{(C_i - C_t)}{r} \tag{3}$$

Where q_t [mg nitrate/g charcoal] is the amount of nitrate removed at time t, C_i [mg nitrate/L] is the initial nitrate concentration, C_t [mg nitrate/L] is the nitrate concentration remaining in the liquid phase of the batch system at time *t* and *r* is the solid-liquid ratio (30 $g.L^{-1}$). The experimental data were fitted with pseudo-first-order and pseudo-second-order kinetic models.

Isotherm of Nitrate Removal by ***C*Zn800***.* The adsorption isotherm data were calculated with equation (4):

$$q_e = \frac{(C_i - C_e)}{r} \tag{4}$$

Where q_e [mg nitrate/g charcoal] is the amount of nitrate removed at equilibrium, C_i [mg nitrate/L] is the initial nitrate concentration, C_e [mg nitrate/L] is the remaining nitrate concentration in the batch system at equilibrium and *r* is the solid-liquid ratio (0.15 g

charcoal / 0.005 L solution). The experimental data of the adsorption isotherms were fitted with both Langmuir and Freundlich models, which are represented by equations (5) and (6) respectively.

$$q_e = \frac{K_L C_e}{1 + K_L C_e} \tag{5}$$

$$q_e = K_F C_e^{1/n} \tag{6}$$

3. Results

The experiments conducted provided data on the synthesis of **C*M800** materials and how these materials remove nitrate from water.

3.1 Synthesis of C*M800

The synthesis (*i.e.*, the conversion process of **C*** to **C*M800**) was characterized by the yield, which is defined as the mass of product formed per 100 g of **C***, by the mass of solid incorporated into the particles, and by the mass loss of the carbonaceous support (Δm).

The yield of the conversion process from **C*** to **C*M800** is shown in **Figure 2**. The highest yield was obtained in the preparation of **C*Al800** (101.4%), followed by **C*Fe800** (41.4%), which is slightly higher than **C*Mg800** (40.7%), and finally **C*Zn800** (33.5%). Interestingly, three out of four syntheses yielded less than 100%.

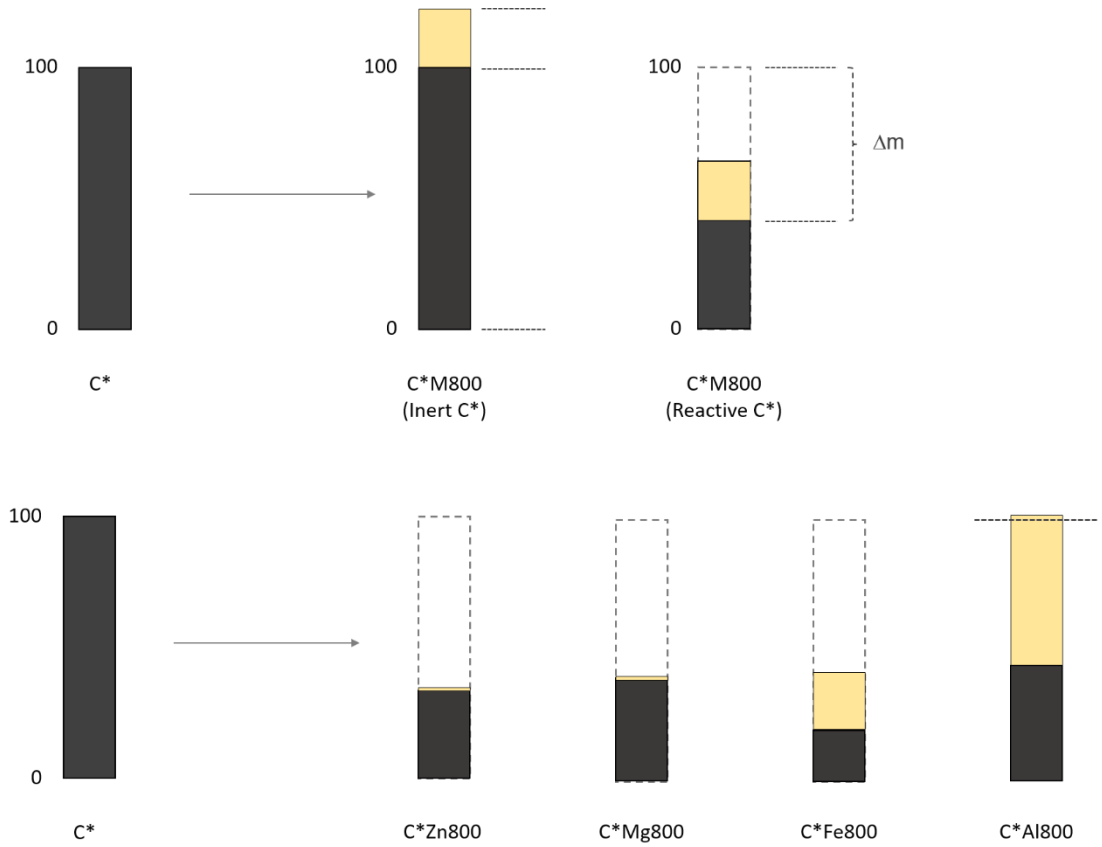

Figure 2. (Top) The column height on the right side schematically represents the yield obtained in a process where the charcoal used in wet impregnation is either inert or reactive. The part of the product corresponding to the oxide formed is indicated in yellow and the part corresponding to the carbonaceous matrix is indicated in dark gray. Δm is the mass loss of C*. (Bottom) Schematic representation of the yields of C*M800 (height of columns) showing the oxide part (yellow) and the carbonaceous matrix (dark gray).

The amount of solid material incorporated during the synthesis was estimated from the percentage of ash obtained after calcination of **C*M800**. **C*Al800** has the highest amount of solid material (56.6%), followed closely by **C*Fe800** (53.1%). With considerably less material, **C*Zn800** (4.1%) and **C*Mg800** (3.1%) show the lowest solid addition.

The amount of mass lost by C* during synthesis was calculated using Equation X. The amount of mass lost by **C*** during synthesis was calculated using equation (1). The maximum ∆m is observed in **C*Fe800** (80.6%), then a lower ∆m is observed in **C*Zn800** (67.9%) and **C*Mg800** (60.6%), and finally, the lowest ∆m is observed in **C*Al800** (55.8%).

In addition to characterizing the synthesis, we have also characterized the materials produced in terms of their structure (SEM, Hg porosimetry) and composition (EDX, XRD).

Figures 2a-d show scanning electron microscopy images of the **C*M800** materials. These images display a distinct way of incorporating solid in each material. **C*Al800** exhibits two main characteristics. Particles locate in some of the macropore mouths, which partially block communication between the macropores and the outside, as evidenced by the space between the macropore walls and the solid particles. Also, solid particles are absent in some macropore mouths and the interior of some macropores. **C*Fe800**, which contains slightly less solid material than **C*Al800**, exhibits a distinct distribution of solid material. In **C*Fe800**, the solid material primarily forms sub- and micrometer particles (with the latter generally smaller than 5 microns) that are evenly distributed on the internal and external surfaces of the charcoal particles, which act as a support. **C*Mg800**, the material that incorporated the least amount of solid, has a similar material distribution to **C*Al800** in that it has solid material in some macropore mouths and lacks particulate material within macropores. However, unlike **C*Al800**, **C*Mg800** has micrometer particles decorating the outer edges of the macropores and blocked macropore entrances. **C*Zn800**, which contains a slightly higher amount of solid material than **C*Mg800**, is unique in that it presents challenges in identifying the location of the incorporated solid material during synthesis. Only a few small micrometer particles are visible, which might be attributed to the solid material incorporated with the synthesis.

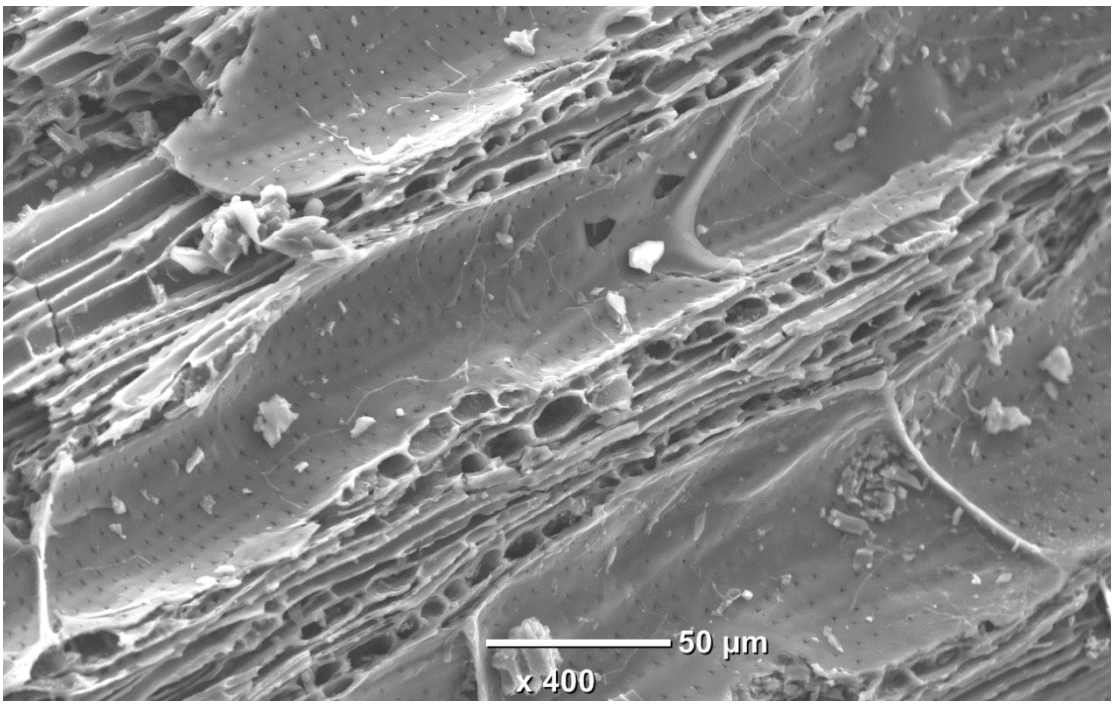

Figure 2a. Scanning electron microscopy images of **C*Zn800**.

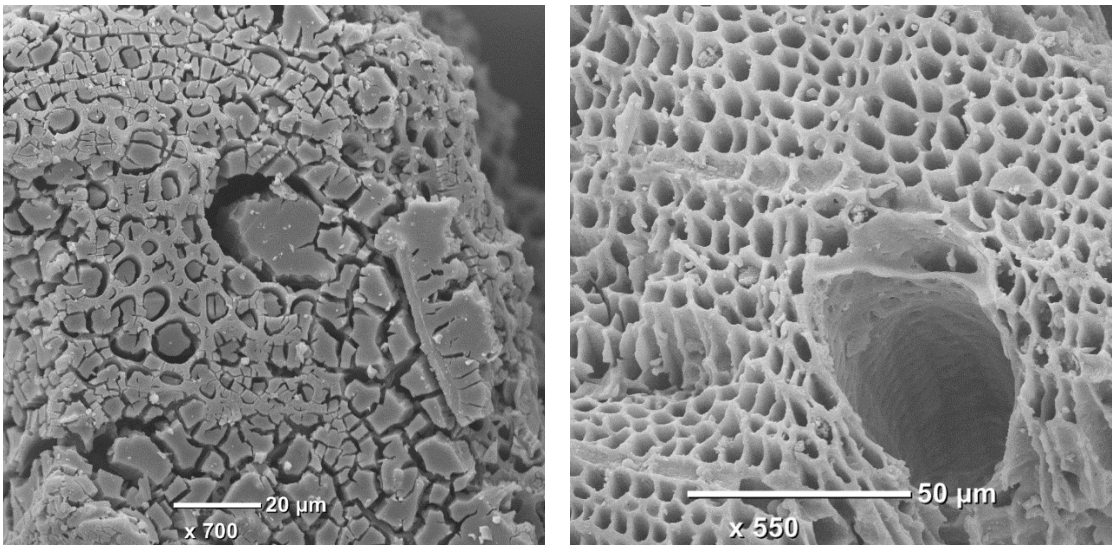

Figure 2b. Scanning electron microscopy images of **C*Al800** with solid material partially blocking macropore entrance (left) and empty macropores (right).

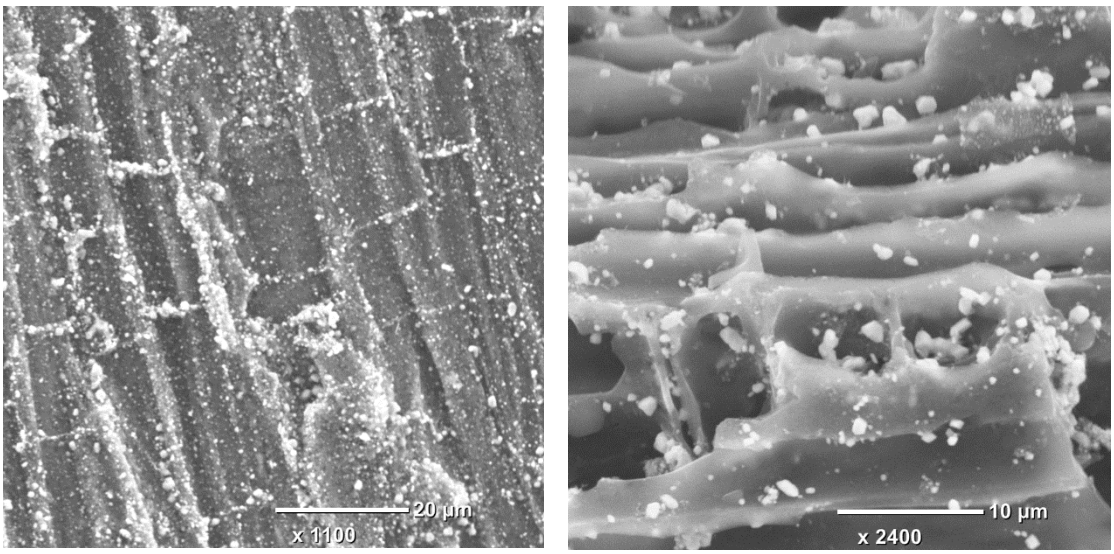

Figure 2c. Scanning electron microscopy images of **C*Fe800** with solid particulate material sub- and micrometersized onto the surface of macropores.

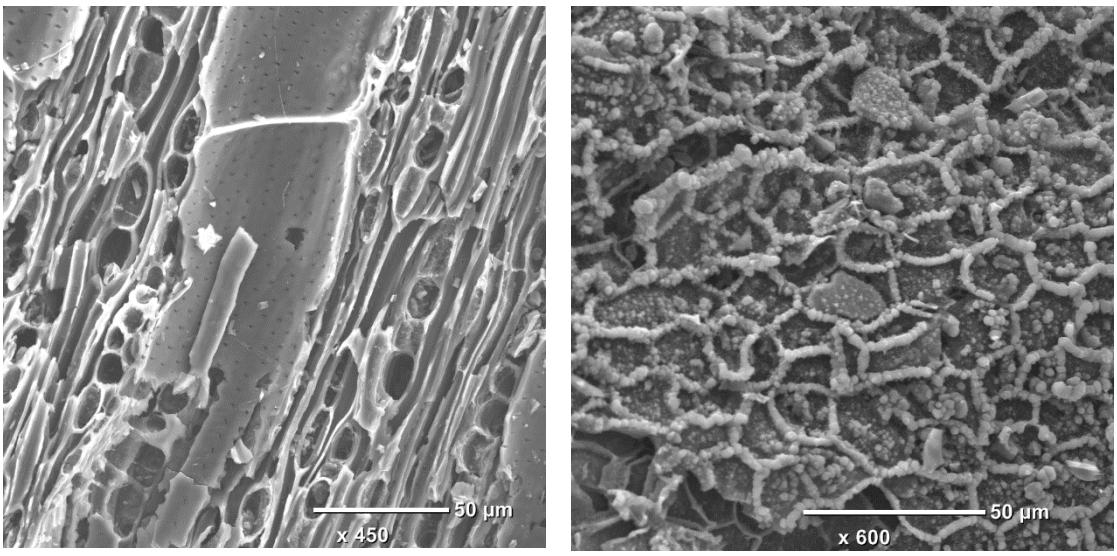

Figure 2d. Scanning electron microscopy images of **C*Mg800** with empty macropores (left) and with micrometersized particles formed at the entrance of macropores (right).

The pore size distribution of **C*M800** was estimated using Hg porosimetry data (see SI). The calculated pore size distributions indicate that all materials have macropores with mean diameters that peaked at 0.05-0.1 and 3-5 microns.

The X-ray diffractograms of the **C*M800** solid materials are shown in **Figure 3**. According to Figure 3, the X-ray diffractograms of **C*M800** solid materials reveal the presence of crystalline phases in **C*Al800** and **C*Fe800**. On the other hand, **C*Mg800** contains only a small amount of crystalline phase, while **C*Zn800** does not show any crystals.

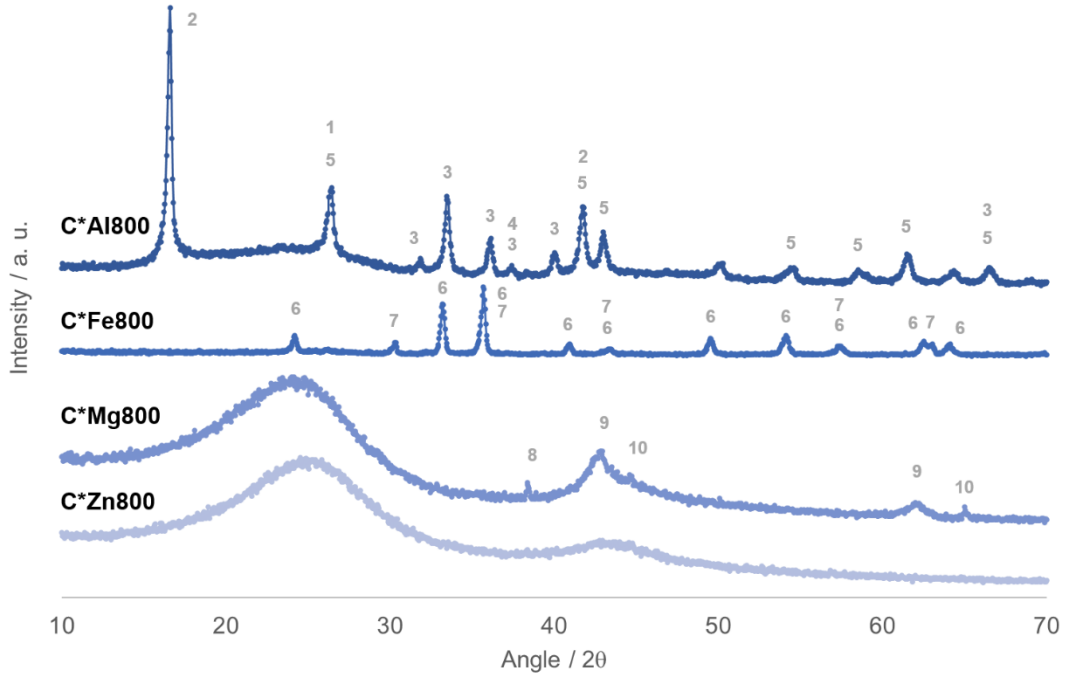

Figure 3. X-ray diffractograms of C*M800 materials. Cliftonite (1) (Ref. Code: 00-041-1487 ICSD), Adamantane (2) (Ref. Code: 00-021-1553 ICSD), Aluminum Oxide (3) (Ref. Code: 00-010-0414 ICSD), Calcium Oxide (4) (Ref. Code: 00-037-1497 ICSD), Aluminum Acetate Hydroxide (5) (Ref. Code: 00-013-0833 ISCD), Iron Oxide (6) (Ref. Code: 01-073-2234 ICSD), Maghemite (7) (Ref. Code: 03-025-1402 ICSD), Magnesium Oxide (8) (Ref. Code: 00-030-0794 ICSD), Periclase (9) (Ref. Code: 01-071-1176 ICSD) y Ferrite (10) (Ref. Code: 00-006-0696 ICSD).

Element distribution in **C*M800** was studied using element mapping by X-ray fluorescence (see SI). The obtained element mappings suggest a homogeneous distribution of **M** elements in all **C*M800** materials. However, in **C*Zn800**, the location of M remains unclear.

To summarize, this section presents the results obtained in characterizing the synthesis and its solid products.

3.2 Nitrate Removal by C*M800

After characterizing the synthesis of **C*M800** and the structure and composition of these materials, we continued investigating their water nitrate removal capacity.

At first, we tested their nitrate removal in batch experiments. **Figure 4** shows the nitrate removal by **C*M800** in batch systems. All materials significantly remove nitrate from the water, but only **C*Zn800** reduces the nitrate concentration below 45 ppm (the maximum allowable level for human consumption).

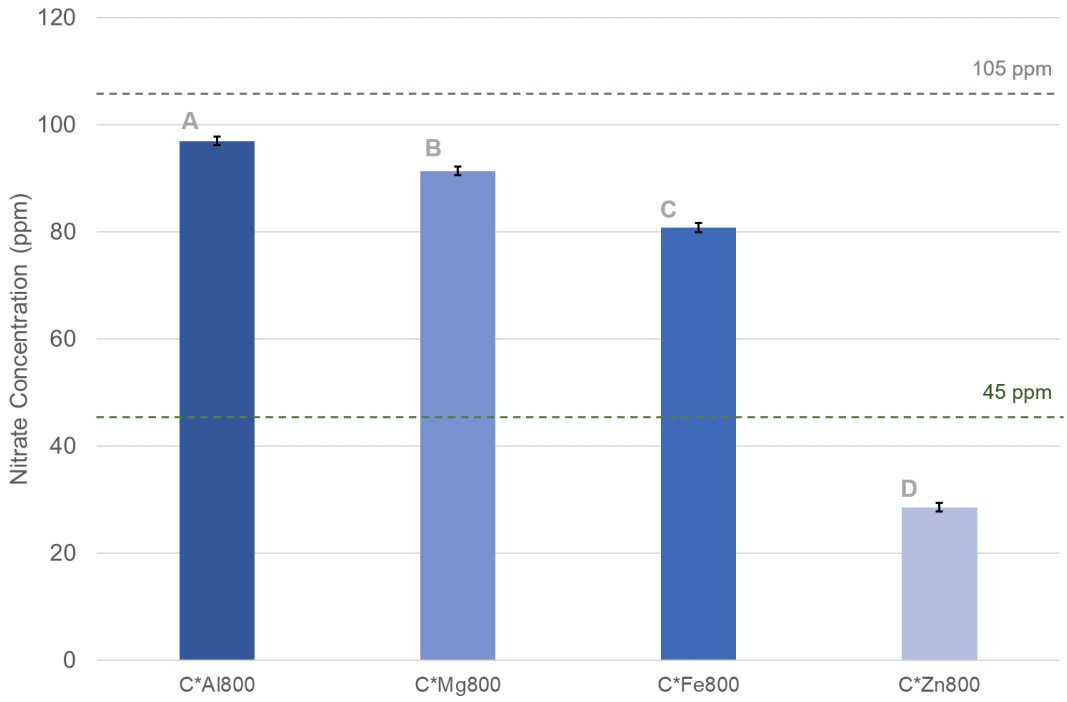

Figure 4. Nitrate concentration in the aqueous phase after treatment in batch system (C_0 = 105 ppm; S/L = 30 $g.L^{-1}$; t = 24 h). Maximum concentration allowed in water according to the World Health Organization: 45 ppm. The error bars represent the confidence interval obtained from the analysis of variance. Different capital letters indicate significantly different means (Tukey test, α=0.05).

Then, we deepened the investigation by studying the kinetics and the removal isotherms of the material **C*Zn800**.

The kinetics of nitrate removal of **C*Zn800** is shown in **Figure 5**. The batch system stabilizes within one hour for the lowest initial nitrate concentration (C_0 = 20 ppm) and within 15 minutes for the highest initial nitrate concentration. The removal kinetics are well described by both pseudo-first order kinetics (R^2 = 0.9185 for C_0 = 20 ppm; R^2 = 0.8986 for C_0 = 2000 ppm) and pseudo-second order kinetics (R^2 = 0.9288 for C_0 = 20 ppm; R^2 = 0.9866 for C_0 = 2000 ppm).

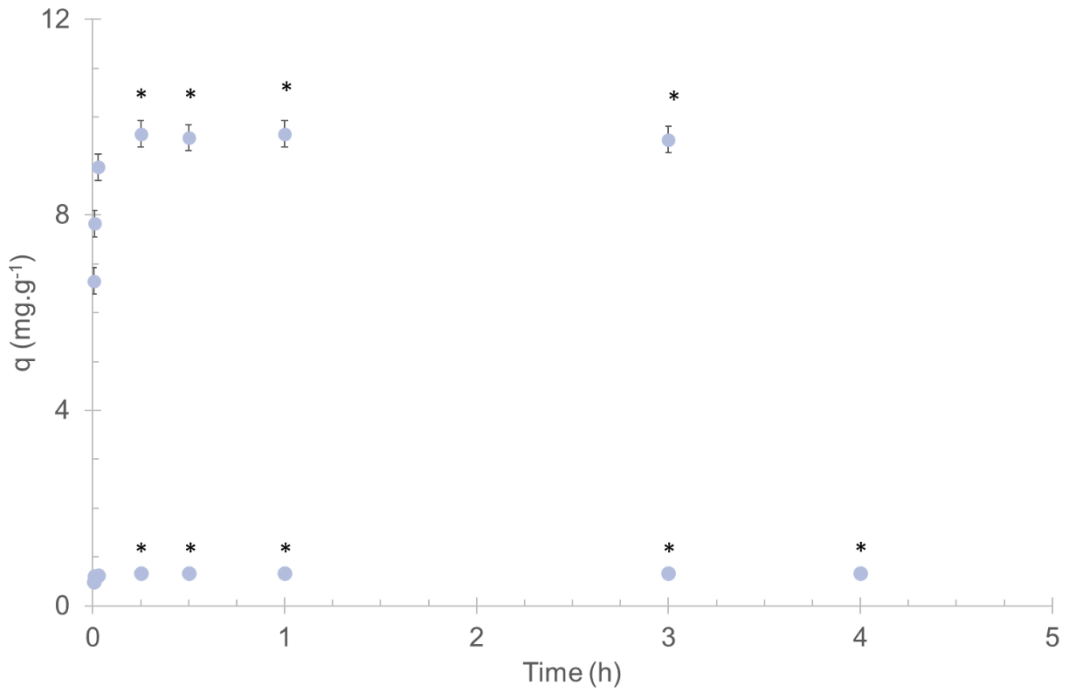

Figure 5. Nitrate removal kinetics of the batch system with **C*Zn800** for initial nitrate concentrations of (a) 20.0 ± 0.2 ppm (bottom) and (b) 2036 ± 4 ppm (top). q is the amount of nitrate (mg) removed per mass unit (g). Error bars represent the confidence interval obtained from the analysis of variance. The absence of asterisks (*) indicates significantly different means (Tukey's test for comparison of means, α=0.05).

The isotherm for nitrate removal was obtained by testing a wide range of initial nitrate concentrations in water (20-2000 ppm) (**Figure 6**). The experimental data fit well with the Freundlich isotherm model (R^2 = 0.9307) and even better with the Langmuir model (R^2 = 0.9943). According to the Langmuir model, **C*Zn800** can remove up to 10.2 mg of nitrate per gram.

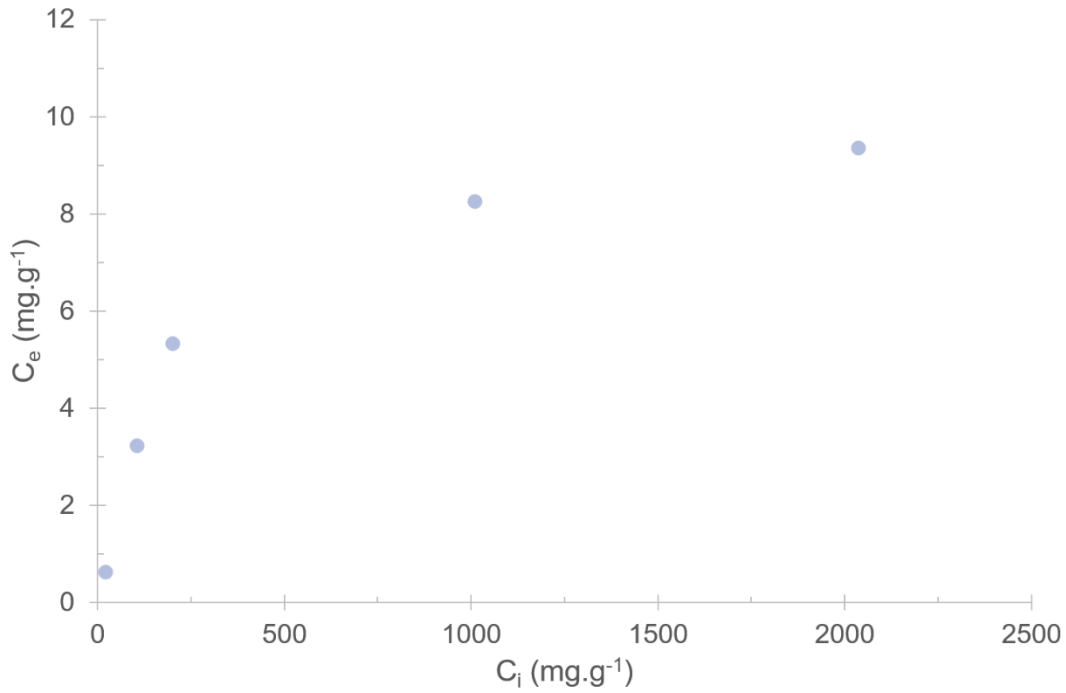

Figure 6. Nitrate removal isotherm of **C*Zn800** (T = 25°C). The circle centered on the mean Ce value covers the error bars of the data (confidence interval obtained from the analysis of variance). All means are significantly different according to Tukey's test (α=0.05). The solid line in dark gray shows the Langmuir isotherm fit.

4. Discussion

In this work, we have investigated the synthesis of oxides supported on charcoal via wet impregnation (**C*M800**) and the use **C*M800** in the removal of nitrate anion from water. Our hypothesis was that we would add oxides (of aluminum, iron, magnesium or zinc) via wet impregnation to form **C*M800** and that **C*M800** would remove better nitrate from water that the material without oxides. Our results indicate that the syntheses produced oxides supported onto charcoal, but that the support changes unexpectedly. Additionally, all **C*M800** materials remove nitrate from water, but only **C*Zn800** removes nitrate more effectively than the material without added oxide.

4.1 Synthesis of C*M800

The first hypothesis of this work was that we could incorporate M metal oxides (M = Al, Fe, Mg, and Zn) into **C*** by wet impregnation. This work´s results indicate that the synthesis forms oxides into charcoal, but surprisingly, the matrix undergoes a significant transformation during the synthesis.

Oxides form in charcoal in a precursor-dependent manner. The precursors had a marked and complex influence on the amount of solid material incorporated, its distribution on the support´s surface, and their crystallinity.

The amount of solids present in **C*M800** varies between two extremes. At one end are **C*Al800** (56.6%) and **C*Fe800** (53.1%). At the other end are **C*Mg800** (3.1%) and **C*Zn800** (4.1%).

The distribution of the solid formed on the support varies from precursor to precursor. **C*Fe800** appears to have a large number of sub- and micrometer particles distributed throughout the pores of the carbonaceous support. **C*Al800** and **C*Mg800**, which incorporated substantially different amounts of material, appear to have the material

mainly in the mouths of some macropores. **C*Zn800** incorporated the solid in such a way that we were unable to see the solid particles in SEM images.

The crystallinity of the particulate material supported onto charcoal also depends on the precursor. **C*Al800** and **C*Fe800** contain crystalline metal oxides, **C*Mg800** seems to have a small amount of magnesium oxide, and **C*Zn800** apparently lacks crystals. These results suggest the absence of correlation between crystallinity and either the mass of the incorporated solid or its distribution onto the support.

The formation of particles supported on charcoal backs the first hypothesis of this work. However, incorporating this solid material caused a significant transformation of the carbonaceous matrix that served as a support.

The carbonaceous support used in the synthesis, C*, loses a significant fraction of its mass. The biggest loss of mass occurs in the synthesis of C*Fe800 (80.6%), in between values for C*Zn800 (67.9%) and C*Mg800 (60.6%), and the minimum mass loss for C*Al800 (54.6%). Considering these mass losses, it is noteworthy that the support keeps its macroporous structure.

This mass loss, while the support maintains its porous structure, indicates that charcoal is chemically active. This chemical activity of the charcoal weakens the idea that it acts as a physical support (while chemical reactions occur in the pores) and strengthens the idea that the support is a reactive component involved in particle formation during wet impregnation.

In addition, this mass loss suggests that the support experiences chemical changes, including breaking and forming new chemical bonds, releasing chemical species (including entire portions of the solid as nanoparticles), and restructuring chemical groups at the surface. These surface groups determine the chemical behavior of the material. Therefore, we can infer that the loss of mass is likely to result in a change in the chemical behavior of the carbonaceous support.

The loss of mass experienced by the carbonaceous support seems to be outside the focus of interest of the scientific community investigating the use of wet impregnation synthesis to synthesize oxides supported on charcoal. In these syntheses, some researchers have implicitly considered the substrate modification when reporting, for instance, changes in specific surface area or pore size distribution (see [10], [11], [12]). However, they seem to omit quantifying the mass loss experienced by charcoal. Quantifying the mass loss from the elemental composition of the support before the reaction and the product is difficult. Quantifying the mass loss requires also knowing how much solid is in the product. Moreover, a reduction in the percentage of carbon does not necessarily correlate with a mass loss of carbonaceous support, as adding oxide particles to an inert carbonaceous support also results in a drop in the carbon content (see for instance [13]).

In short, our experimental data support the first hypothesis of this work. The wet impregnation of C* allows synthesizing a composite material with M-metal oxide supported on carbon. However, it is worth mentioning that our data additionally shows that the carbonaceous support experiences a considerable transformation during the synthesis.

4.2 Nitrate Removal

The second hypothesis of this work was that C*M800 materials would perform better than **C*800** (*i.e.*, the material that experienced the same process except the wet impregnation). This work´s results show that the hypothesis finds experimental support for only one **C*M800** material.

Only **C*Zn800** outperforms **C*800** [14] in removing nitrate in batch systems. While the latter reduces the nitrate concentration to a level above the maximum allowable concentration for human consumption, the former reduces the nitrate concentration to a

safe value for human consumption. Furthermore, C*Zn800 performs similarly to other charcoal-supported zinc oxides reported in the literature [13], [15], [16], [17].

C*Fe800, **C*Mg800**, and **C*Al800,** though significantly remove nitrate from water, they underperform compared to **C*800**. Moreover, they seem to underperform compared to other charcoal-supported iron-oxides [18], [19] and magnesium-oxides [20] and aluminum-oxides [21], [22], [23] reported in the literature. Compared to those materials, the poor performance of **C*M800** (M = Al, Fe, Mg) suggests that fine-tuning the synthesis variables may be needed to improve their ability to remove nitrate from water.

4.3 Outlook

This work demonstrates the complexity of synthesizing oxide particles supported on porous charcoal via wet impregnation.

The amount of incorporated oxide, pore material distribution, and crystallinity varied significantly from precursor to precursor. This influence suggests that the precursor provides a knob for fine-tuning the properties of the product. Other knobs for fine-tuning the product are synthesis parameters such as carbonaceous supports and reaction temperatures and times.

The changes experienced by the carbonaceous support suggest the need to investigate how changes in the carbonaceous support affect nitrate removal from water. Nitrate removal from water depends on the chemical groups present in the material —the chemical groups of the incorporated solid and those of the carbonaceous support. Therefore, investigating the influence of the support on nitrate removal could provide a new perspective for developing oxide-carbon composite materials for water filtration.

5. Conclusion

In summary, our study demonstrates that the incorporation of oxides through wet impregnation is a synthesis route that enables the production of a material that outperforms the material without the addition of oxide in removing nitrate from water. The incorporation of solid material via wet impregnation introduces modifications in the charcoal used as support, resulting in a synergistic effect in material synthesis.

Acknowledgments

This study was supported by CONICET (PIP2013-0105, Long´s PhD fellowship) and ANPCYT (PICT-2014-2583).

Authors' Contribution

Long A. Leonel: Methodology, Investigation, Formal analysis, Visualization, Writing - Review & Editing.

Arnal Pablo M.: Conceptualization, Methodology, Investigation, Formal analysis, Visualization, Writing – Original Draft, Review & Editing, Supervision, Project administration, Funding acquisition [24].

References

[1] W. B. Jensen, “The Lewis Acid-Base Definitions: A Status Report,” *Chem Rev*, vol. 78, no. 1, 1978, doi: 10.1021/cr60311a002.

[2] S. Khandaker, Y. Toyohara, S. Kamida, and T. Kuba, “Adsorptive removal of cesium from aqueous solution using oxidized bamboo charcoal,” *Water Resour Ind*, vol. 19, pp. 35–46, Jun. 2018, doi: 10.1016/J.WRI.2018.01.001.

[3] M. M. Saleh, “On the removal of cationic surfactants from dilute streams by granular charcoal,” *Water Res*, vol. 40, no. 5, pp. 1052–1060, 2006, doi: 10.1016/j.watres.2005.12.032.

[4] M. F. Chowdhury, S. Khandaker, F. Sarker, A. Islam, M. T. Rahman, and M. R. Awual, “Current treatment technologies and mechanisms for removal of indigo carmine dyes from wastewater: A review,” *Journal of Molecular Liquids*, vol. 318. Elsevier B.V., Nov. 15, 2020. doi: 10.1016/j.molliq.2020.114061.

[5] S. Khandaker, M. F. Chowdhury, M. R. Awual, A. Islam, and T. Kuba, “Efficient cesium encapsulation from contaminated water by cellulosic biomass based activated wood charcoal,” *Chemosphere*, vol. 262, p. 127801, Jan. 2021, doi: 10.1016/J.CHEMOSPHERE.2020.127801.

[6] D. Kalderis *et al.*, “Bamboo-derived adsorbents for environmental remediation: A review of recent progress,” *Environ Res*, vol. 224, p. 115533, May 2023, doi: 10.1016/J.ENVRES.2023.115533.

[7] M. Zhang *et al.*, “Evaluating biochar and its modifications for the removal of ammonium, nitrate, and phosphate in water,” *Water Research*, vol. 186. Elsevier Ltd, Nov. 01, 2020. doi: 10.1016/j.watres.2020.116303.

[8] L. A. Long and P. M. Arnal, “Conversion of Wood into Hierarchically Porous Charcoal in the 200-Gram-Scale Using Home-Built Kiln,” ChemRXiv. Accessed:

Jul. 06, 2022. [Online]. Available: https://chemrxiv.org/engage/chemrxiv/article-details/60c757084c8919accbad4938

[9] L. A. Long and P. M. Arnal, “Affinity for Anions Developed in Charcoal by Acid Treatment,” Jul. 2022, doi: 10.26434/CHEMRXIV-2022-X3LSC.

[10] N. Gao, K. Chen, and C. Quan, “Development of CaO-based adsorbents loaded on charcoal for CO2 capture at high temperature,” *Fuel*, vol. 260, 2020, doi: 10.1016/j.fuel.2019.116411.

[11] S. S. Shah, I. Ahmad, and W. Ahmad, “Adsorptive desulphurization study of liquid fuels using Tin (Sn) impregnated activated charcoal,” *J Hazard Mater*, vol. 304, 2016, doi: 10.1016/j.jhazmat.2015.10.046.

[12] F. F. de Brites-Nóbrega, A. N. B. Polo, A. M. Benedetti, Mô. M. D. Leão, V. Slusarski-Santana, and N. R. C. Fernandes-Machado, “Evaluation of photocatalytic activities of supported catalysts on NaX zeolite or activated charcoal,” *J Hazard Mater*, vol. 263, 2013, doi: 10.1016/j.jhazmat.2013.07.061.

[13] A. Bhatnagar *et al.*, “Removal of nitrate from water by adsorption onto zinc chloride treated activated carbon,” *Sep Sci Technol*, vol. 43, no. 4, pp. 886–907, Mar. 2008, doi: 10.1080/01496390701787461.

[14] L. A. Long and P. M. Arnal, “Affinity for Anions Developed in Charcoal by Acid Treatment,” *ChemRxiv*, Nov. 2022, doi: 10.26434/CHEMRXIV-2022-X3LSC-V2.

[15] M. A. Khan *et al.*, “Adsorption Studies for the Removal of Nitrate Using Modified Lignite Granular Activated Carbon,” *http://dx.doi.org/10.1080/01496395.2011.601782*, 2011, doi: 10.1080/01496395.2011.601782.

[16] L. Liu, M. Ji, and F. Wang, “Adsorption of Nitrate onto ZnCl2-Modified Coconut Granular Activated Carbon: Kinetics, Characteristics, and Adsorption Dynamics,”

Advances in Materials Science and Engineering, vol. 2018, 2018, doi: 10.1155/2018/1939032.

[17] A. Rezaee, H. Godini, S. Dehestani, and A. Khavanin, “Application of Impregnated Almond Shell Activated Carbon by Zinc Sulfate for Nitrate Removal from Water,” *J. Environ. Health. Sci. Eng.*, vol. 5, no. 2, pp. 125–130, 2008.

[18] G. Tan, Y. Mao, H. Wang, and N. Xu, “A comparative study of arsenic(V), tetracycline and nitrate ions adsorption onto magnetic biochars and activated carbon,” *Chemical Engineering Research and Design*, vol. 159, pp. 582–591, Jul. 2020, doi: 10.1016/j.cherd.2020.05.011.

[19] N. Mehrabi, M. Soleimani, M. M. Yeganeh, and H. Sharififard, “Parameter optimization for nitrate removal from water using activated carbon and composite of activated carbon and Fe2O3 nanoparticles,” *RSC Adv*, vol. 5, no. 64, pp. 51470–51482, 2015, doi: 10.1039/c5ra03920g.

[20] M. Zhang, B. Gao, Y. Yao, Y. Xue, and M. Inyang, “Synthesis of porous MgO-biochar nanocomposites for removal of phosphate and nitrate from aqueous solutions,” *Chemical Engineering Journal*, vol. 210, pp. 26–32, 2012, doi: 10.1016/j.cej.2012.08.052.

[21] A. Bhatnagar, E. Kumar, and M. Sillanpää, “Nitrate removal from water by nano-alumina: Characterization and sorption studies,” *Chemical Engineering Journal*, vol. 163, no. 3, pp. 317–323, Oct. 2010, doi: 10.1016/j.cej.2010.08.008.

[22] N. Abbas, F. Deeba, M. Irfan, M. Tahir Butt, N. Jamil, and R. A. Khan, “Treatability Study of Arsenic, Fluoride and Nitrate from Drinking Water by Adsorption Process,” *J.Chem.Soc.Pak*, vol. 36, no. 5, 2014, [Online]. Available: https://www.researchgate.net/publication/275223078

[23] B. Kasprzyk-Hordern, “Chemistry of alumina, reactions in aqueous solution and its application in water treatment,” *Advances in Colloid and Interface Science*, vol. 110, no. 1–2. pp. 19–48, Jun. 30, 2004. doi: 10.1016/j.cis.2004.02.002.

[24] L. Allen, A. O’Connell, and V. Kiermer, “How can we ensure visibility and diversity in research contributions? How the Contributor Role Taxonomy (CRediT) is helping the shift from authorship to contributorship,” *Learned Publishing*, vol. 32, no. 1. Wiley-Blackwell, pp. 71–74, Jan. 01, 2019. doi: 10.1002/leap.1210.